JOURNAL OF SOLID STATE CHEMISTRY 109, 134–144 (1994)

The Effect of Oxygen Stoichiometry on Phase Relations and Structure in the System $La_{1-x}Sr_xFeO_{3-\delta}$ ($0 \leq x \leq 1$, $0 \leq \delta \leq 0.5$)

S. E. Dann, D. B. Currie, and M. T. Weller[1]

Department of Chemistry, University of Southampton, Highfield, Southampton, SO9 5NH United Kingdom

and

M. F. Thomas and A. D. Al-Rawwas

Oliver Lodge Laboratory, University of Liverpool, Liverpool, L69 3BX United Kingdom

Received January 22, 1993; in revised form July 13, 1993; accepted July 16, 1993

An extensive range of compounds in the $La_{1-x}Sr_xFeO_{3-\delta}$ ($0 \leq x \leq 1$, $0 \leq \delta \leq 0.5$) system have been synthesized. When $\delta \approx 0$ the system is composed of three crystallographically different regions: orthorhombic for $0 \leq x \leq 0.2$, rhombohedral for $0.4 \leq x \leq 0.7$, and cubic for $0.8 \leq x \leq 1.0$. Products were characterized by thermogravimetric analysis and Mössbauer spectroscopy yielding information on oxygen stoichiometry and iron oxidation state. At 4.2 K, Mössbauer spectra are composed of magnetic sextet components arising from different charge states of iron; in the orthorhombic and rhombohedral phases the charge states Fe^{3+} and Fe^{5+} coexist, and Fe^{4+} and Fe^{3+} are present in the cubic region. Room temperature Mössbauer spectra show that samples in the orthorhombic region are still magnetically ordered and the coexistence of Fe^{3+} and Fe^{5+} remains, while between $x = 0.4$ and $x = 1.0$ the samples are paramagnetic; in the rhombohedral region the spectra show the presence of Fe^{4+} and Fe^{3+}, and in the cubic region both Fe^{4+} and an intermediate valence state are assigned. High-resolution powder neutron diffraction data were collected on samples annealed under high-pressure oxygen, and full structure refinements were carried out using the Rietveld method. Accurate bond length data obtained for all phases show that the iron coordination geometry becomes more regular with increasing Sr, and hence Fe^{4+}, content. A phase diagram for the full range of lanthanum/strontium and oxygen stoichiometry is proposed.

INTRODUCTION

The perovskite series $La_{1-x}Sr_xFeO_{3-\delta}$ ($0 \leq x \leq 1$) was first studied by Waugh (1), who observed complex phase changes from orthorhombic at low x through rhombohedral to cubic as the stoichiometry approached $SrFeO_3$ ($\delta = 0$). Since the distortions were very small, no further structural information was obtained by Waugh although the complex magnetic properties of these materials were soon after investigated by Kelly (2). Preliminary Mössbauer measurements were undertaken by Shimony and Knudsen (3); at high values of x, characteristic Fe^{4+} lines were observed with an isomer shift relative to that of ^{57}Co in stainless steel of 0.1 to 0.2 mm sec^{-1}. Lower values of x, however, gave broad and varying linewidths which were attributed to an intermediate Fe^{3+}/Fe^{4+} valence state.

Previous Mössbauer studies have revealed complex behavior in the oxides of iron(IV). $SrFeO_3$ (4) is a metallic conductor with a Neel temperature of 134 K which remains cubic down to 4.2 K, showing a single magnetic hyperfine sextet with a flux density (B) of 33.1 T and an isomer shift (δ_{IS}) of 0.146 mm sec^{-1}. The absence of Jahn–Teller distortion in this high spin $3d^4$ state was explained by the high electrical conductivity where the e_g^* orbitals are broadened into an itinerant electronic conduction band. The structurally related material $CaFeO_3$ (5) however, exhibits very different Mössbauer behavior with a pair of hyperfine split sextets of equal intensity at 4.2 K with the Mössbauer parameters $B_1 = 41.6$ T, $\delta_{IS} = 0.34$ mm sec^{-1}, and $B_2 = 27.9$ T, $\delta_{IS} = 0.00$ mm sec^{-1}. On heating, the two signal sets merge initially into two singlets of equal intensity above 116 K and finally into a singlet at 300 K. These observations were interpreted as a change from a paramagnetic Fe^{4+} state to a mixed valence Fe^{3+}/Fe^{5+} state as indicated in the charge disporportionation

$$2Fe^{4+} \rightleftharpoons Fe^{3+} + Fe^{5+}.$$

Above the Neel temperature of 116 K, $CaFeO_3$ is a paramagnetic mixed valence material which becomes

[1] To whom correspondence should be addressed.

0022-4596/94 $6.00

antiferromagnetically ordered below 116 K, retaining mixed valence. This behavior is not observed in $SrFeO_3$, although the mean values of the Mössbauer parameters are very similar. No structural evidence to support this ordering behavior in $CaFeO_3$ has been observed even at low temperature.

Takano *et al.* (6, 7) studied the $La_{1-x}Sr_xFeO_{3-\delta}$ and $Ca_{1-x}Sr_xFeO_{3-\delta}$ systems using Mössbauer spectroscopy. Lattice constants were defined for $x = 0.4$, 0.5, 0.7, 0.8, and 0.9 ($0 < \delta < 0.05$), but no further structural determination was attempted. Takano has proposed a nonintegral oxidation state of iron in these materials following disproportionation of the type

$$2Fe^{4+} \rightleftharpoons Fe^{4-\lambda} + Fe^{4+\lambda} \quad (0 \leq \lambda \leq 1).$$

These compounds were shown to behave in a similar way in the Mössbauer as $CaFeO_3$.

The most recent study to be performed on a compound in the $La_{1-x}Sr_xFeO_{3-\delta}$ system was by Battle *et al.* (8). This series of compounds $LaSr_2Fe_3O_{9-y}$ ($0 < y \leq 1$), equivalent to $x = 0.66$ using our notation, was investigated using a variety of annealing techniques and characterized by powder X-ray and neutron diffraction. Mössbauer measurements showed the same disproportionation reaction as that seen in $CaFeO_3$. However, the expected reduction in symmetry due to this ordering was not observed by either diffraction technique below the transition temperature. Takano had already suggested an explanation for this in his previous work on $CaFeO_3$ when he proposed that the phenomenon was only a very short-range ordering effect and therefore not monitorable by a bulk technique such as diffraction.

This paper describes the preparation of a range of samples in the $La_{1-x}Sr_xFeO_{3-\delta}$ series ($0 \leq x \leq 1$), ($0 \leq \delta \leq 0.5$) using a variety of annealing techniques, and their characterization by powder X-ray diffraction. Samples annealed under high-pressure oxygen were also investigated using powder neutron diffraction on HRPD at the Rutherford Appleton Laboratory. Mössbauer data were collected on these samples to correlate the disproportionation behavior with the structural changes observed. Oxygen content was measured by thermogravimetric analysis.

EXPERIMENTAL

Samples in the series $La_{1-x}Sr_xFeO_{3-\delta}$ ($0 \leq x \leq 1$) were prepared by direct solid state reaction of $SrCO_3$ (99.9%), Fe_2O_3 (99.995%), and La_2O_3 (99.99%) mixed in the correct molar proportions in a pestle and mortar, and initially fired at 1100°C in air. After regrinding, the samples were reheated to 1300°C for another 24 hr and compounds were then treated further to control the oxygen stoichiometry as defined in Table 1.

TABLE 1

Sample	Annealing gas	Treatment
A	Air	Quenched from 1300°C
B	1% O_2/N_2	Annealed at 480°C overnight, slow cooled to RT
C	O_2	Annealed at 480°C overnight, slow cooled to RT
D	5%H_2/N_2	Annealed at 800°C overnight, slow cooled to RT
E	Ar	Annealed at 480°C overnight, slow cooled to RT
F	High-pressure O_2	Annealed at 900°C/350 atm flowing O_2, slow cooled

X-ray powder diffraction data were collected using a Siemens D5000 diffractometer fitted with primary monochromator operating with Cu$K\alpha_1$ radiation. A stepped scan using a step size of 0.002° and long collection times were employed in an attempt to resolve the small structural distortions.

Oxygen content was measured by thermogravimetric analysis using a Stanton Redcroft TG 1000 thermobalance operating up to 800°C under an atmosphere of 5% H_2/N_2 and platinum crucibles.

Mössbauer data were collected on the high-pressure annealed samples between 4.2 K and room temperature using a conventional transmission spectrometer using a double ramp waveform to give a flat background. Absorbers were prepared of finely ground samples, which were weighed to give optimum signal to noise (9), mixed with boron nitride to randomize the orientations of the microcrystals. Sources of up to 100 mCi of ^{57}Co in Rh were used and the spectrometers were calibrated using α-iron at room temperature. Isomer shifts were determined relative to α-iron at 300 K.

Powder neutron diffraction data were obtained on HRPD at the Rutherford Appleton Laboratory on the high pressure oxygen annealed samples for all of x. Data collection times varied from 3 to 4 hr. Full profile refinements were carried out using a time of flight version of the Rietveld method (10). Although the samples $x = 0.0$ to 0.3 are below their Neel temperature at 298 K, the maximum d spacing used for the refinement was 1.7 Å below which magnetic reflections are extremely weak and could be ignored. Refinements were carried out in the space group $Pbnm$, $x = 0.0$–0.2, $R\bar{3}c$ for $x = 0.4$ to 0.7 and $Pm3m$ for $x = 0.8$ to 1.0 using the starting models of $GdFeO_3$ (11), $LaCuO_3$ (12), and $SrFeO_3$ (13) for the three space groups, respectively. Refinement included all atomic positions, cell parameters, scale factors, background, and peak shapes. Oxygen stoichiometry was permitted to vary for all samples initially but was finally fixed for samples $x = 0.0$ to 0.7 as the stoichiometry varied

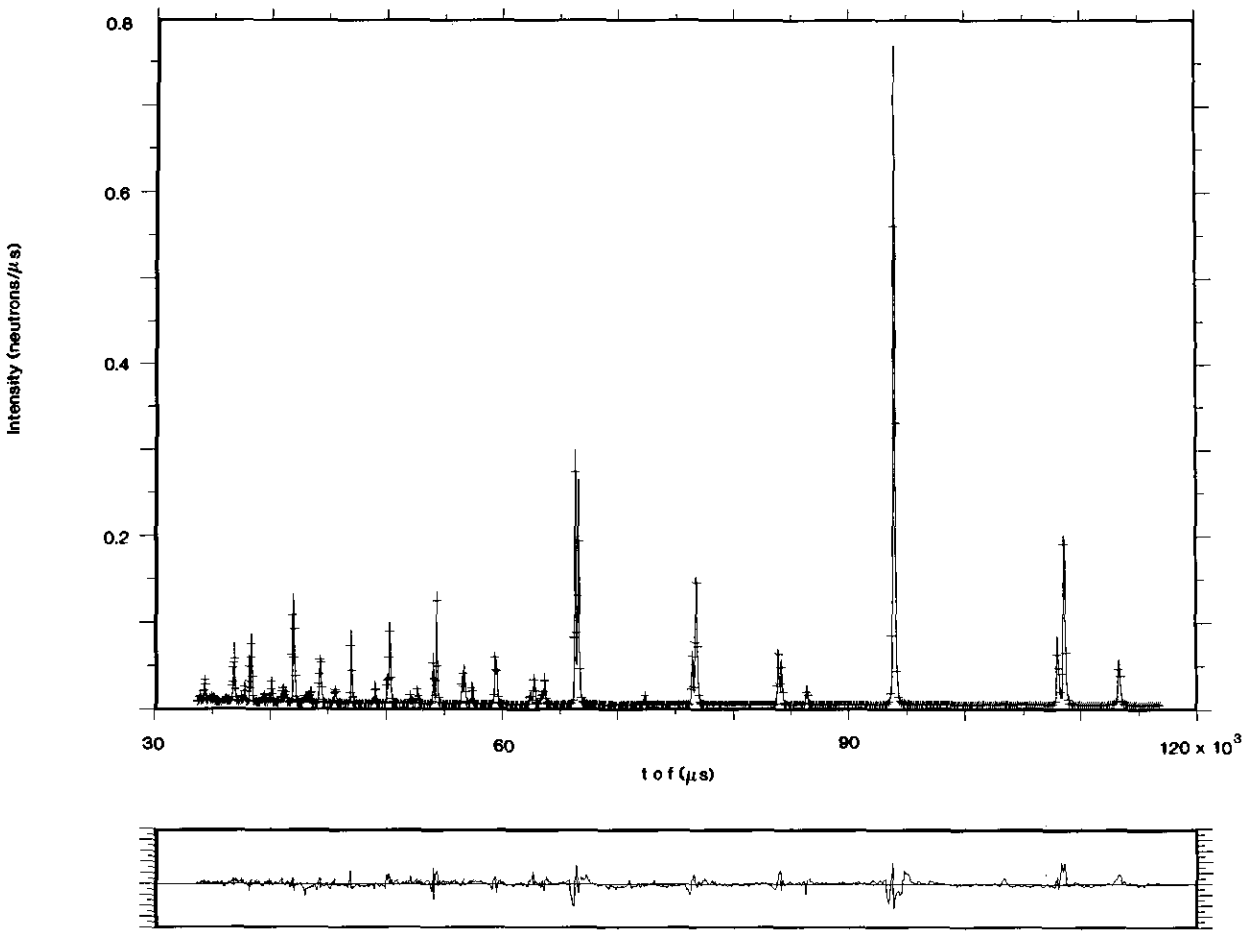

FIG. 1. Representation of the fit to the HRPD data for $x = 0.5$. The lower broken line represents the experimental data and the upper solid line, the calculated pattern. The fit is represented in the lower box on a smaller scale.

only marginally from three and always within the ESD. Final stages of the refinements included anisotropic temperature factors. A typical fit to the HRPD data is shown in Fig. 1.

RESULTS

Annealing Experiments

The annealing experiments revealed complex phase relations in the $La_{1-x}Sr_xFeO_{3-\delta}$ system. As first observed by Waugh (1), the system is composed of three regions of different symmetry at low values of δ. However, as demonstrated by Battle *et al.* (8) in the $Sr_2LaFe_3O_{9-y}$ system, the purity and symmetry of this system shows extreme sensitivity to oxygen stoichiometry and sample preparation, especially at high values of x. A summary of the annealing experiments, including refined lattice parameters, oxygen content determined by thermogravimetric analysis, and space group are included in Table 2.

Similar behavior is also apparent in the $SrFeO_{3-\beta}$ system, where the value of β is very sensitive to both sample preparation and annealing conditions. The $SrFeO_{3-\beta}$ system has been studied extensively by many authors (14–17), and many different phases have been recognized in the system; Machesney *et al.* reported the presence of both a cubic ($\beta = 0$) and tetragonal ($\beta = 0.14$) phase. At higher values of β several orthorhombic phases have been reported; Greaves and co-workers (18) reported a phase in which, when $\beta = 0.25$, every other oxygen site was vacant in the 110 direction, and this is related to the pure brownmillerite phase, $Sr_2Fe_2O_5$ (19), where all these sites are vacant.

Recent studies have further investigated the low symmetry phases, and a variety of conclusions have been reached depending on the sample preparation method. Takeda *et al.* (20) produced a whole range of complex phases from a preparation technique involving quenching from high temperature. Lower temperature experiments performed by Yamauchi and co-workers (21) produced more ordered samples of higher symmetry. Location of phase boundaries thus varied according to preparative conditions.

TABLE 2
Results from Annealing Experiments (x = 0.0–0.9)

Gas	0.0	0.1	0.2	0.3	0.4	0.5	0.6	0.7	0.8	0.9
A	*Pbnm*	*Pbnm*	*Pbnm*		$R\bar{3}c$	$R\bar{3}c$				
	5.5553(8)	5.556(3)	5.550(2)		5.5271(6)	5.519(3)				
	5.5663(8)	5.539(3)	5.508(2)	Mixture	13.4209(18)	13.421(8)	Mixture	Mixture	Mixture	Mixture
	7.8545(13)	7.856(5)	7.844(5)		$\delta = 0$	$\delta = 0$				
	$\delta = 0$	$\delta = 0$	$\delta = 0$							
B		*Pbnm*	*Pbnm*		$R\bar{3}c$					
		5.558(3)	5.551(4)		5.5286(4)				3.881(2)	3.8785(9)
		5.538(3)	5.508(4)	Mixture	13.4202(9)	Mixture	Mixture	Mixture	3.861(2)	3.8581(10)
		7.850(5)	7.844(4)		$\delta = 0$				$\delta = 0.12$	$\delta = 0.16$
		$\delta = 0$	$\delta = 0$							
C		*Pbnm*	*Pbnm*		$R\bar{3}c$	$R\bar{3}c$				
		5.566(2)	5.549(2)		5.5283(4)	5.516(2)				3.8688(2)
		5.540(2)	5.514(2)	Mixture	13.4206(8)	13.417(4)	Mixture	Mixture	Mixture	3.8566(8)
		7.858(2)	7.841(3)		$\delta = 0$	$\delta = 0$				$\delta = 0.12$
		$\delta = 0$	$\delta = 0$							
D	*Pbnm*	*Pbnm*	*Pbnm*	*Pm3m*	*Pm3m*					
	5.5752(8)	5.564(3)	5.557(3)	3.9175(2)	3.9151(4)					
	5.5640(8)	5.553(2)	5.540(3)	$\delta = 0.15$	$\delta = 0.20$	Mixture	Mixture	Mixture	Mixture	Mixture
	7.8563(12)	7.852(4)	7.846(7)							
	$\delta = 0.0$	$\delta = 0.05$	$\delta = 0.10$							
E		*Pbnm*	*Pbnm*		$R\bar{3}c$					
		5.556(6)	5.552(6)		5.5304(6)			3.8948(6)	3.8836(6)	
		5.540(2)	5.520(2)	Mixture	13.4272(13)	Mixture	Mixture	3.8613(6)	3.8542(6)	Mixture
		7.855(3)	7.841(2)		δ 0.08			$\delta = 0.12$	$\delta = 0.16$	
		$\delta = 0$	$\delta = 0$							
F		*Pbnm*	*Pbnm*		$R\bar{3}c$	$R\bar{3}c$	$R\bar{3}c$	$R\bar{3}c$	*Pm3m*	*Pm3m*
		5.556(2)	5.550(2)		5.5269(2)	5.5093(8)	5.4945(1)	5.4767(6)	3.8610(13)	3.8556(3)
		5.535(2)	5.512(3)	Mixture	13.4209(6)	13.4121(14)	13.4108(14)	13.4049(5)	$\delta = 0.03$	$\delta = 0.04$
		7.848(3)	7.844(4)		$\delta = 0$	$\delta = 0$	$\delta = 0$	$\delta = 0$		
		$\delta = 0$	$\delta = 0$							

Described below is the effect of different annealing conditions on the $La_{1-x}Sr_xFeO_{3-\delta}$ system.

x = 0.0 to 0.2. At these low values of strontium substitution, full oxygen stoichiometry is maintained within the limits of experimental error except during the reduction experiment. The symmetry of the samples remained *Pbnm* throughout the experiments although the orthorhombic distortion decreased slightly on reduction. In the high pressure oxygen annealed samples the orthorhombic distortion increases from x = 0.0 to 0.2, and this is reflected in the changing bond distances around the iron metal center, *vide infra*.

x = 0.3. Initial examination of the x = 0.3 sample by X-ray diffraction showed it to be multiphase for all annealing experiments except the reduction. Close scrutiny of the XRD patterns showed a mixture of both rhombohedral and orthorhombic phases. Reduction of the 0.3 phase in hydrogen gave a phase which showed sharp reflections and no peak splitting or additional reflections to suggest a noncubic unit cell, and was hence indexed on a primitive cubic unit with a cell parameter of 3.9175(4) Å.

x = 0.4 to 0.7. The rhombohedral region shows a much wider range of oxygen nonstoichiometry and consequently more complex phase relations. The high pressure annealed samples exhibited the clearest distortions which were clearly visible for samples x = 0.4 to 0.6 by X-ray diffraction. The x = 0.7 sample at first appeared cubic, although reflections were clearly broadened at high angles. The neutron diffraction experiment showed the sample to be rhombohedral with a very small $a\sqrt{6}/c$ distortion of 1.0008. The other annealing experiments gave differing results depending on the value of x.

For x = 0.4 the system remained rhombohedral through the entire range of annealing experiments except the reduction where a phase change to pseudo-cubic occurred. δ remained very small (0 ± 0.03) when oxygen was present but increased to 0.08 in the argon annealing experiment with a corresponding increase in both cell parameters. The reduction produced a similar phase to the reduced x = 0.3 sample which was indexed as primitive cubic with a cell parameter of 3.9151(4) Å.

In the x = 0.5 sample, only high-pressure oxygen an-

nealing and 100% oxygen of 1 atmosphere produced a pure rhombohedral phase. The other experiments, excluding the reduction, produced a mixture of orthorhombic and rhombohedral phases. The reduction experiment produced a mixture of an orthorhombic $(A,B)_3Fe_3O_8$ phase, as first observed by Grenier *et al.* (22) and also observed by Battle *et al.* (23), and the cubic 0.4 phase.

A similar mixture of phases is observed when $x = 0.6$, except the multiphase region extends to the tube furnace oxygen annealed sample. The only pure rhombohedral phase was produced by the high-pressure experiment.

For $x = 0.7$ a pure rhombohedral phase was only produced by the high pressure experiment. The other three annealing techniques employing oxygen produced a mixture of orthorhombic and tetragonal phases as observed for $SrFeO_{3-\beta}$ ($\beta = 0.27$). However, argon annealing produced a pure tetragonal phase similar to that observed by many authors in $SrFeO_{2.78-2.86}$. The main phase from the reduction experiment was $Sr_2LaFe_3O_8$ with a small amount of the reduced 0.4 phase.

$x = 0.8$ to 0.9. The last region produced the most complex systems of all due to the wide range of oxygen nonstoichiometry. At $x = 0.8$ a cubic phase was produced by the high-pressure experiment, with both the oxygen-annealed and the as-sintered samples being a mixture of tetragonal and cubic phases. Both the oxygen in nitrogen and the argon-annealed products were pure tetragonal phases. The hydrogen reduction gave a complex mixture of $Sr_2LaFe_3O_8$ and $Sr_2Fe_2O_5$.

For $x = 0.9$ very similar properties are observed to those described above, except the oxygen annealed sample was also tetragonal. Both the reduction and the argon experi-

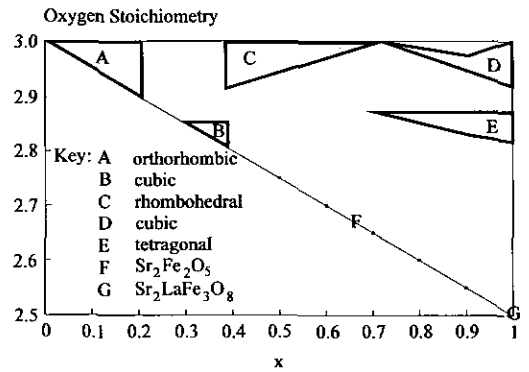

FIG. 2. The diagram represents a phase diagram which describes the full range of x and δ. The labeled regions are identified in the key, while the unlabeled regions are multiphase.

TABLE 3
Refined Lattice Parameters and Bond Lengths for the Orthorhombic Region $x = 0.0$ to 0.2

x	Lattice parameters	Atomic parameters: Atom	x/a	y/b	z/c	B_{eq}	Occ	Bond distances: La–O	Fe–O	Refinement parameters
0	a = 5.55702(2)	La	0.9923(4)	0.0292(1)	0.25	0.52(1)	1.0	O1$^+$ 3.059(2) × 1	O1$^\bullet$ 2.009(1) × 2	$R_p = 2.33$
	b = 5.56521(1)	Fe	0	0	0	0.73(1)	1.0	O1$^\bullet$ 2.581(2) × 1	O2* 2.002(1) × 2	
	c = 7.85426(2)	O1	0.0748(4)	0.4855(3)	0.25	0.37(2)	1.0	O1° 3.152(2) × 1	O2$^+$ 2.010(1) × 2	$R_{wp} = 3.37$
		O2	0.7191(2)	0.2817(2)	0.0394(1)	0.35(1)	1.0	O1* 2.421(3) × 1		
								O2$^\times$ 2.648(2) × 2		$R_{exp} = 1.62$
								O2$^\diamond$ 2.805(1) × 2		
								O2$^\triangle$ 3.277(1) × 2		$\chi^2 = 4.33$
								O2$^\blacksquare$ 2.450(2) × 2		
0.1	a = 5.55561(2)	La	0.9940(11)	0.0200(5)	0.25	0.45(5)	0.9	O1$^+$ 2.934(6) × 1	O1$^\bullet$ 2.004(1) × 2	$R_p = 5.76$
	b = 5.53540(2)	Sr	0.9940(11)	0.0200(5)	0.25	0.45(5)	0.1	O1$^\bullet$ 2.668(6) × 1	O2* 2.026(3) × 2	
	c = 7.85609(6)	Fe	0	0	0	0.15(4)	1.0	O1° 3.144(9) × 1	O2$^+$ 1.961(3) × 2	$R_{wp} = 9.23$
		O1	0.0714(12)	0.4958(10)	0.25	0.57(9)	1.0	O1* 2.419(9) × 1		
		O2	0.7194(6)	0.2724(5)	0.0373(4)	0.32(6)	1.0	O2$^\times$ 2.659(5) × 2		$R_{exp} = 2.64$
								O2$^\diamond$ 2.825(4) × 2		
								O2$^\triangle$ 3.202(5) × 2		$\chi^2 = 12.24$
								O2$^\blacksquare$ 2.465(5) × 2		
0.2	a = 5.55002(12)	La	0.9964(20)	0.0121(9)	0.25	0.30(6)	0.8	O1$^+$ 2.725(13) × 1	O1$^\bullet$ 1.994(1) × 2	$R_p = 13.92$
	b = 5.51209(9)	Sr	0.9964(20)	0.0121(9)	0.25	0.30(6)	0.2	O1$^\bullet$ 2.840(13) × 1	O2* 2.030(5) × 2	
	c = 7.84394(17)	Fe	0	0	0	0.19(8)	1.0	O1° 3.118(13) × 1	O2$^+$ 1.930(5) × 2	$R_{wp} = 18.6$
		O1	0.0653(13)	0.5016(21)	0.25	0.36(6)	1.0	O1* 2.433(13) × 1		
		O2	0.7261(7)	0.2612(10)	0.0356(5)	0.26(8)	1.0	O2$^\times$ 2.639(08) × 2		$R_{exp} = 5.59$
								O2$^\diamond$ 2.865(08) × 2		
								O2$^\triangle$ 3.109(07) × 2		$\chi^2 = 11.89$
								O2$^\blacksquare$ 2.502(07) × 2		

TABLE 4
Refined Lattice Parameters and Bond Lengths for the Rhombohedral Region $x = 0.4$ to 0.7

x	Lattice parameters	Atomic parameters						Bond distances		Refinement parameters
		Atom	x/a	y/b	z/c	B_{eq}	Occ	La–OX	Fe–OX	
0.4	a = 5.52728(1)	La	0	0	0.25	0.31(3)	0.6	O$X^{\bullet}$ 2.997(2) × 3	O$X^{\bullet}$ 1.963(1) × 6	R_p = 7.34
	c = 13.42116(4)	Sr	0	0	0.25	0.31(3)	0.4	O$X^{\blacksquare}$ 2.530(1) × 3		R_{wp} = 8.86
		Fe	0	0	0	0.12(4)	1.0	OX^{+} 2.758(1) × 6		R_{exp} = 3.41
		OX	0.4577(2)	0	0.25	0.68(3)	1.0			χ^2 = 10.16
0.5	a = 5.51107(1)	La	0	0	0.25	0.28(3)	0.5	O$X^{\bullet}$ 2.947(2) × 3	O$X^{\bullet}$ 1.963(1) × 6	R_p = 5.39
	c = 13.41578(2)	Sr	0	0	0.25	0.28(3)	0.5	O$X^{\blacksquare}$ 2.564(1) × 3		R_{wp} = 6.87
		Fe	0	0	0	0.25(2)	1.0	OX^{+} 2.751(1) × 6		R_{exp} = 2.89
		OX	0.4651(1)	0	0.25	0.63(2)	1.0			χ^2 = 5.66
0.6	a = 5.493671(1)	La	0	0	0.25	1.26(4)	0.4	O$X^{\bullet}$ 2.894(2) × 3	O$X^{\bullet}$ 1.946(1) × 6	R_p = 8.13
	c = 13.41057(4)	Sr	0	0	0.25	1.26(4)	0.6	O$X^{\blacksquare}$ 2.600(1) × 3		R_{wp} = 10.75
		Fe	0	0	0	1.08(1)	1.0	OX^{+} 2.745(1) × 6		R_{exp} = 3.17
		OX	0.4733(2)	0	0.25	1.47(4)	1.0			χ^2 = 10.73
0.7	a = 5.47623(1)	La	0	0	0.25	1.74(8)	0.3	O$X^{\bullet}$ 2.811(2) × 3	O$X^{\bullet}$ 1.937(1) × 6	R_p = 6.45
	c = 13.40551(4)	Sr	0	0	0.25	1.74(8)	0.7	O$X^{\blacksquare}$ 2.665(2) × 3		R_{wp} = 9.30
		Fe	0	0	0	1.54(2)	1.0	OX^{+} 2.738(1) × 6		R_{exp} = 3.07
		OX	0.4867(3)	0	0.25	1.89(7)	1.0			χ^2 = 9.21

ment gave a mixture of $Sr_2LaFe_3O_8$ and $Sr_2Fe_2O_5$. A summary of the phase behavior is shown in Fig. 2. The data for the $x = 1.0$ series were taken from the results described by Yamauchi and co-workers (21).

Neutron Diffraction Experiments

The neutron diffraction refinements of the orthorhombic samples proceeded steadily in the space group *Pbnm*. In the case of $x = 0.0$ and $x = 0.1$ some additional magnetic reflections just below 1.7 Å had to be removed from the refinement. The final sample in this group was the most difficult to refine, and close examination of the diffraction data showed misfitting on the low time of flight tail of some of the reflections. This is probably due to the fact that this sample lies on the border of the phase transition from orthorhombic to rhombohedral, and that the likely cause of the misfitting is the presence of a small amount of the rhombohedral phase. Despite the impurity, for which due to overlap exclusion of peaks was not possible, both atomic positions and cell parameters were steady and remained within the ESDS. Final refinement parameters and important bond lengths and angles are listed in Table 3.

A multiphase refinement program was not available at the time of data collection and so the refinement of the HRPD data for the $x = 0.3$ sample was not possible. The rhombohedral phases refined rapidly in the space group $R\bar{3}c$ although the peak shape parameters were very difficult to fit in the case of $x = 0.6$ and 0.7 due to the small rhombohedral distortions giving rise to very small peak splittings. Final refinement parameters and important bond lengths are listed in Table 4.

The two cubic samples were refined in the space group *Pm3m*. Although 0.8 proceeded smoothly, the 0.9 sample showed significant peak broadening and was more difficult

TABLE 5
Refined Lattice Parameters and Bond Lengths for the Cubic Region $x = 0.8$ to 0.9

x	Lattice parameters	Atomic parameters						Bond distances		Refinement parameters
		Atom	x/a	y/b	z/c	B_{eq}	Occ	La–O	Fe–O	
0.8	3.86434(1)	La	0	0	0	0.36(1)	0.2	O$^{\bullet}$ 2.733(1) × 12	O$^{\bullet}$ 1.932(1) × 6	R_p = 8.41
		Sr	0	0	0	0.36(1)	0.8			R_{wp} = 9.64
		Fe	0.5	0.5	0.5	0.10(1)	1.0			R_{exp} = 4.91
		O	0	0.5	0.5	0.67(1)	1.00(1)			χ^2 = 3.86
0.9	3.85609(1)	La	0	0	0	0.27(4)	0.1	O$^{\bullet}$ 0.727(1) × 12	O$^{\bullet}$ 1.928(1) × 6	R_p = 13.92
		Sr	0	0	0	0.27(4)	0.9			R_{wp} = 18.61
		Fe	0.5	0.5	0.5	0.01(4)	1.0			R_{exp} = 5.59
		O	0	0.5	0.5	0.47(4)	0.99(3)			χ^2 = 10.99

TABLE 6
Mössbauer Parameters at 4.2 K

	Fe^{3+}				Fe^{4+}				Fe^{5+}				
x	IS (mm sec^{-1})	B_{hf} (kG)	QS (mm sec^{-1})	Int (%)	IS (mm sec^{-1})	B_{hf} (kG)	QS (mm sec^{-1})	Int (%)	IS (mm sec^{-1})	B_{hf} (kG)	QS (mm sec^{-1})	Int (%)	Calculated oxygen content
0.0	0.47	562	—	100									3.00
0.1	0.45	560	−0.09	57					0.06	264	−0.02	9	3.04
	0.42	539	−0.06	34									
0.2	0.47	560	−0.09	35					−0.05	264	0	11	3.01
	0.43	537	−0.05	54									
0.3	0.48	555	−0.04	16					−0.04	267	−0.02	16	3.01
	0.43	528	−0.06	68									
0.4	0.41	534	−0.04	33					−0.04	271	−0.04	21	3.01
	0.41	506	−0.09	46									
0.5	0.44	521	−0.05	22					−0.02	272	−0.05	27	3.02
	0.40	492	−0.06	51									
0.6	0.38	487	−0.02	26					−0.03	262	0	30	3.00
	0.37	466	−0.05	44									
0.7	0.37	466	−0.03	24					−0.01	266	−0.04	35	3.00
	0.35	452	−0.03	41									
0.8	0.33	456	−0.06	11	0.18	337	—	71					2.96
	0.32	430	−0.06	18									
0.9	0.39	447	0.06	12	0.17	333	—	88					2.99
1.0					0.07	326		100					3.00

to refine. However, no additional reflections were observed to suggest a lower symmetry. Close scrutiny of the neutron diffraction pattern shows a high-angle tail which could be attributed to a $SrFeO_3$ impurity. Final refinement parameters and important bond lengths are listed in Table 5.

Experimentally determined Mössbauer parameters for the high-pressure annealed samples at 4.2 K and room temperature are summarized in Tables 6 and 7. The calculated oxygen content determined from the relative proportions of the integrated iron signals is included. An example of the Mössbauer spectrum for all three crystallographi-

TABLE 7
Mössbauer Parameters at 298 K

	Fe^{3+}				Fe^{4+}				Fe^{5+}				
x	IS (mm sec^{-1})	B_{hf} (kG)	QS (mm sec^{-1})	Int (%)	IS (mm sec^{-1})	B_{hf} (kG)	QS (mm sec^{-1})	Int (%)	IS (mm sec^{-1})	B_{hf} (kG)	QS (mm sec^{-1})	Int (%)	Calculated oxygen content
0.0	0.37	523	−0.08	100									3.00
0.1	0.38	537	−0.08	45					−0.05	224	0.12		3.00
	0.33	486	−0.03	50								5	
0.2	0.37	512	−0.06	36					−0.07	227	−0.02		3.02
	0.37	421	−0.14	52								12	
0.3	0.36	556	−0.04	5					−0.19	268	−0.02	9	2.94
	0.32	556	−0.04	46.5									
	0.22	528	0.22	39.5									
0.4	0.29		0.12	59	0.10			41					3.00
0.5	0.27		0.10	50	0.09			50					3.00
0.6	0.25		0.08	40	0.10			60					3.00
0.7	0.23		0.06	30	0.09			70					3.00
0.8	0.19		—	28	0.08			72					2.96
0.9	0.18		0.493	13	0.09			87					2.99
1.0					0.07			100					3.00

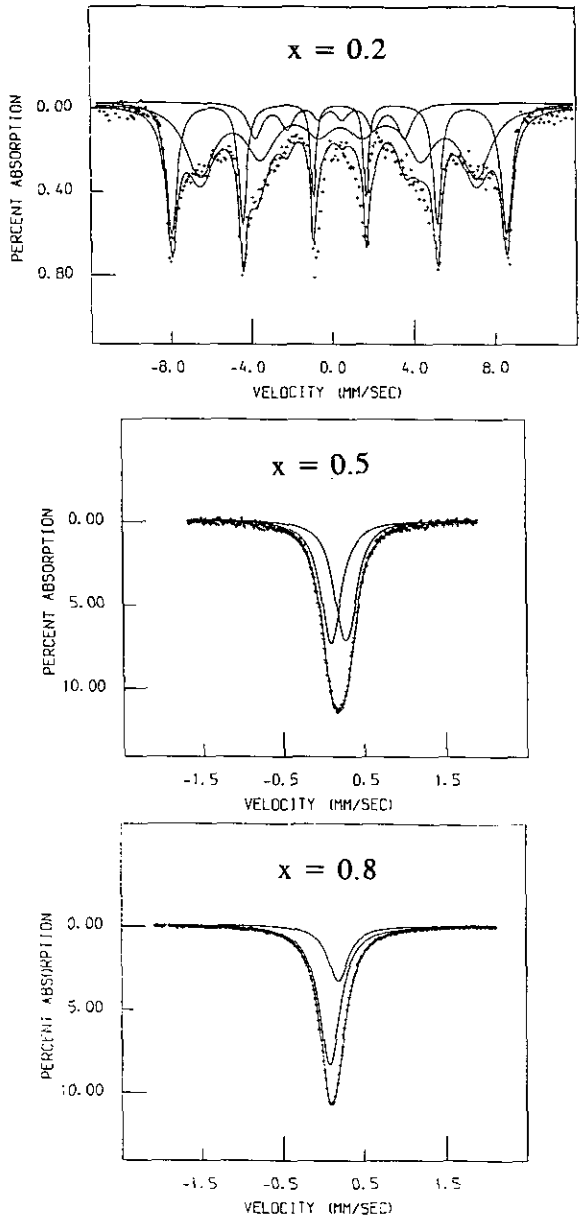

FIG. 3. Example of the Mössbauer data for the three crystallographic regions of the high-pressure oxygen-annealed samples at room temperature.

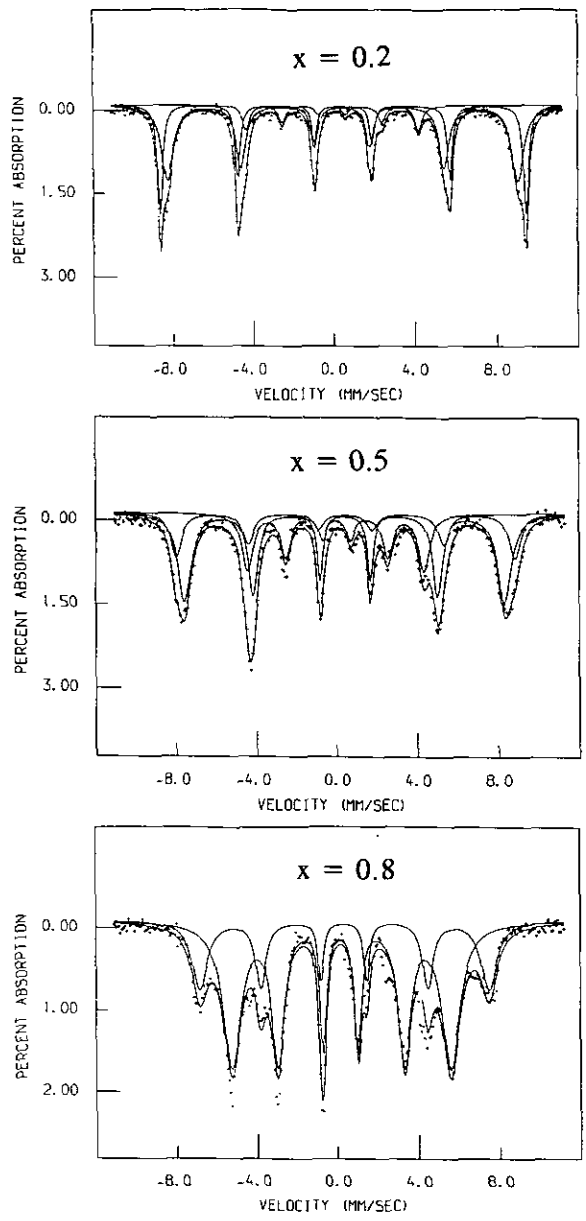

FIG. 4. Example of the Mössbauer data for the three crystallographic regions of the high-pressure oxygen-annealed samples at 4.2 K.

cally distinct regions for these high pressure annealed samples at 4.2 K and room temperature are shown in Figs. 3 and 4.

DISCUSSION

The results from the neutron refinements were in close agreement with those first derived by X-ray diffraction. Oxygen content determined by TGA and neutron diffraction, and those calculated from the relative proportions of iron^{n+}, where $n = 3^+$, 4^+, and 5^+ determined by Mössbauer analysis, were also in very close agreement (± 0.02).

Figures 5 and 6 show the variation in lattice parameter with varying strontium content and a plot of the change in volume with strontium substitution for the high-pressure oxygen-annealed samples. A comparison of the two shows that although the overall volume is changing linearly with x, the local environment of the ions and, hence, individual lattice parameters change significantly. Figure 5 shows that the variation in lattice parameter falls into three distinct regions corresponding to the different crys-

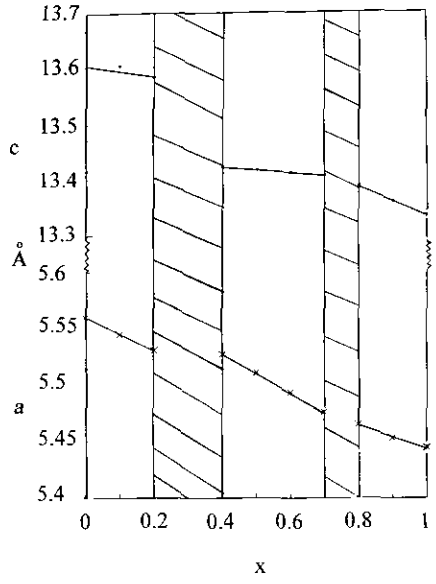

FIG. 5. Variation of lattice parameter with strontium level x in $La_{1-x}Sr_xFeO_{3-\delta}$. (For comparable values for the c parameter, *Pbnm* $c_0\sqrt{3}$ and *Pm3m* $a_c 2\sqrt{3}$, and for the a parameter $a_c\sqrt{2}$.)

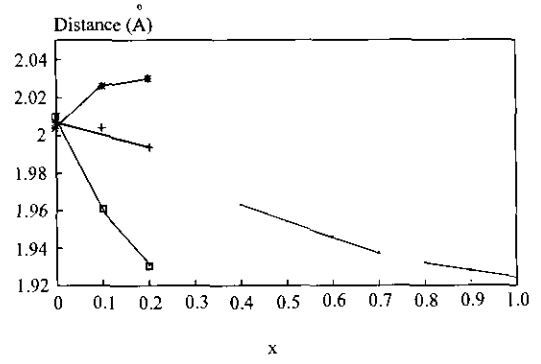

FIG. 7. Variation of iron–oxygen bonding distance with x in $La_{1-x}Sr_xFeO_{3-\delta}$. The attributed symbols are consistent with those given in Tables 3–5.

tal systems. Although the change in lattice parameter within these systems is linear there is a discontinuity at the phase boundaries. The most obvious of these is in the region between 0.2 and 0.4, and perhaps gives an indication as to why the 0.3 sample is multiphase and the 0.2 sample also shows signs of rhombohedral impurity.

A three-region graph is also observed in Figs. 7 and 8, which show the variation in bond length around La/Sr and Fe with strontium substitution for the high-pressure oxygen-annealed samples. The noncontinuity is most obvious between orthorhombic and rhombohedral, but is also present between rhombohedral and cubic. If the La/Sr–O distances are extrapolated by means of a curve to a point where they coincide, i.e., all twelve A cation to oxygen distances are equal as for a cubic system using the rhombohedral region of Fig. 7, a phase change to cubic at $x = 0.8$ is implied, but the rhombohedral distortion graph (Fig. 9) suggests a slightly lower value between 0.72 and 0.73 by linear extrapolation, i.e., $a\sqrt{6}/c$ ratio would equal one for a cubic phase. This would imply a relaxation of the local structure around the La when the structure becomes rhombohedral. The most likely explanation of the observed structural changes is the effect of the changing iron oxidation state as the series is transversed. Clearly there is a change in both ionic size and the oxygen ordering as iron moves from the tripositive to the tetrapositive state. The replacement of lanthanum by strontium is likely to have very little structural impact since they are approximately the same size and prefer similar coordination geometries. Considering the first phase change between $x = 0.2$ and $x = 0.4$, the iron site changes from being a very distorted to an almost regular

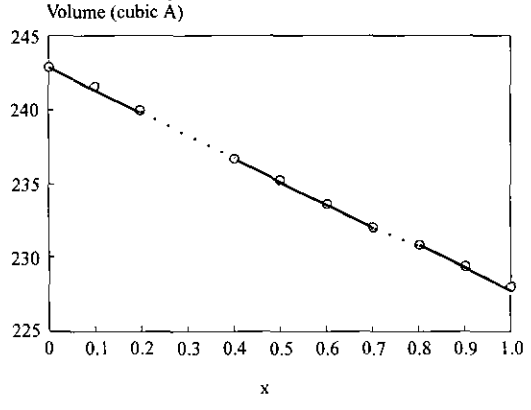

FIG. 6. Variation of cell volume with strontium level x in $La_{1-x}Sr_xFeO_{3-\delta}$. (For comparable values for the c parameter, *Pbnm* $c_0\sqrt{3}$ and *Pm3m* $a_c 2\sqrt{3}$, and for the a parameter $a_c\sqrt{2}$.)

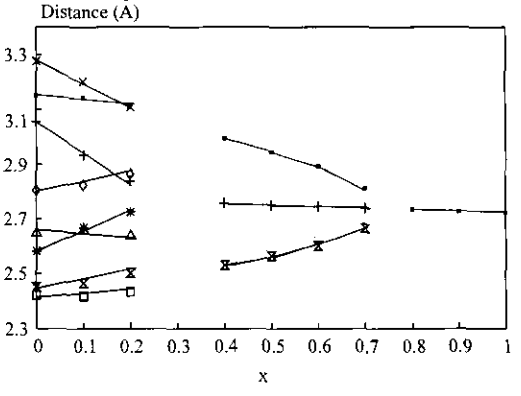

FIG. 8. Variation of strontium/lanthanum–oxygen bond lengths with x in $La_{1-x}Sr_xFeO_{3-\delta}$. The attributed symbols are consistent with those given in Tables 3–5.

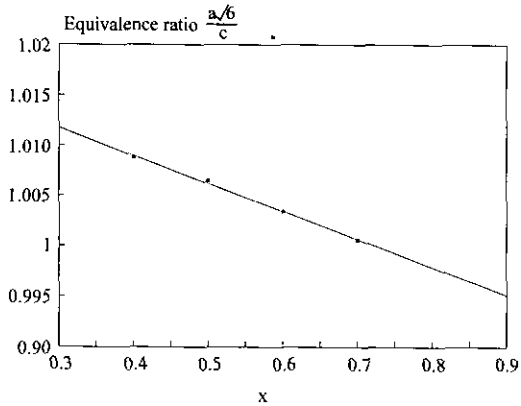

FIG. 9. Variation of a/b ratio for the rhombohedral region in $La_{1-x}Sr_xFeO_{3-\delta}$.

octahedron with equal bond lengths and bond angles only slightly distorted from the idealized 90°, O–Fe–O, of 89.3 and 90.7°. The former situation is a higher unusual environment for both iron oxidation states.

A common way of describing bonding interactions in solids is by the relationship developed by Brown and Aldermatt (24), which relates the valence of a site to its bond lengths. The calculated valence of each iron site is summarized in Table 8. At high values of x the tabulated values show very good agreement. However, at low values of x in the orthorhombic region, the site valence gradually deviates to a greater extent from the theoretical value as x increases from 0.0 to 0.2. This behavior suggests that the iron atom is getting progressively more overbonded. Once the phase change has occurred to rhombohedral symmetry, the good agreement between site valence and expected iron oxidation state determined by TGA is restored. This suggests that the first phase change is probably related to the preferred geometry of iron as its average oxidation state increases. The second phase change from rhombohedral to cubic is more difficult to explain since the difference in the two coordination geometries in the structure is minimal. However, considering the A cation

TABLE 8
Comparison of Calculated Bond Valence and Iron Oxidation State Derived from Compound Stoichiometry

x	Oxidation state	Calculated bond valence
0.0	3.00	3.064
0.1	3.10	3.154
0.2	3.20	3.270
0.4	3.40	3.447
0.5	3.50	3.533
0.6	3.60	3.610
0.7	3.70	3.699
0.8	3.74	3.749
0.9	3.82	3.789

there is a significant difference in the geometry of the 12-fold site. In the cubic case all 12 bond distances are the same, whereas the rhombohedral system has a distorted site. This distortion gradually decreases in the rhombohedral region until there is a changeover to cubic symmetry. This changeover is also reflected in a large drop in the temperature factors, suggesting conversion from a "rattling" ion in an overly large cavity to a more acceptable coordination.

The Mössbauer measurements on the high-pressure oxygen-annealed samples show a clear difference between the rhombohedral/orthorhombic and cubic regions. The rhombohedral region, which has previously been studied using Mössbauer spectroscopy by Takano *et al.* (6, 7) and more recently by Battle *et al.* (8) on the sample $Sr_2LaFe_3O_{8.94}$, shows parameters which are most applicable to Fe^{3+} and Fe^{5+} valance states. At room temperature the rhombohedral spectrum can be interpreted as a mixed valence iron (III) and iron (IV) state which undergoes charge disproportionation at low temperature to give three hyperfine split sextets which are relatively sharp. The sharpness of the signal is indicative of an ordered spin arrangement, and magnetic reflections are indeed observed at low temperature using the POLARIS neutron diffractometer at the Rutherford Appleton Laboratory. However, examination of the nuclear reflections at low temperature did not suggest a reduction in symmetry as a consequence of the disproportionation reaction. The low temperature behavior and magnetic reflections are similar to those observed for $Sr_2LaFe_3O_{8.94}$ (8); however, both POLARIS and D1A have relatively poor resolution, and tiny structural changes would probably not be resolved using these diffractometers. The Mössbauer parameters observed for the rhombohedral and cubic regions are similar to those observed by Takano *et al.* (6, 7) although in our case the best fit to the data was achieved using three iron signals instead of two, which was used by Takano for most of his assignments. Averaged Mössbauer parameters in all cases are in very good agreement with those observed by Takano.

The disproportionation behavior, producing Fe^{3+} and Fe^{5+}, clearly extends to the orthorhombic region although these samples are magnetically ordered at room temperature. Comparison of the 4.2 K spectra with that of the rhombohedral region shows obvious similarities. In contrast to this, the spectrum from the cubic region is very different with Mössbauer parameters characteristic of iron (III) and iron (IV) at 4.2 K. At room temperature the Fe^{4+} component continues to have characteristic iron (IV) parameters, i.e., $\delta \approx 0.09$ mm sec^{-1} but the Fe^{3+} component has a very low isomer shift of $\delta = 0.17$ mm sec^{-1}. The low temperature spectra show similar behavior to that noted for the slightly oxygen-deficient cubic region of $SrFeO_{3-\delta}$ $\delta < 0.05$ (20). The room temperature behavior

can be most easily described by an averaged charge state as first assigned by Takano et al. (6, 7).

Quadrupolar splitting, where there is Fe^{3+}/Fe^{5+} disproportionation, is in all cases very small or negligible, suggesting that the crystallographic site is distorted from octahedral to a very small extent. This observation is in good agreement with the neutron diffraction data which show only a slightly distorted site with bond lengths typically in the range 1.93–2.03 Å for the orthorhombic region and bond angles only slightly removed from 90° in both rhombohedral and orthorhombic regions.

ACKNOWLEDGMENT

We thank the SERC for the studentship for SED.

REFERENCES

1. J. S. Waugh, M.I.T. Lab. for Insulation Res. Technical Report No. 152. (1960).
2. W. F. Kelly, M. S. thesis, M.I.T. (1961).
3. U. Shimony and J. M. Knudsen, *Phys. Rev.* **144,** 361 (1966).
4. T. Takeda, Y. Yamaguchi, and H. Watanabe, *J. Phys. Soc. Jpn.* **33,** 967 (1972).
5. M. Takano, N. Nakanishi, Y. Takeda, S. Naka, and T. Takada, *Mater. Res. Bull.* 12, 923 (1977).
6. M. Takano, J. Kawachi, N. Nakanishi, and Y. Takeda, *J. Solid State Chem.* **39,** 75 (1981).
7. M. Takano and Y. Takeda, *Bull. Inst. Chem. Res., Kyoto Univ.* **61,** 5, 406 (1983).
8. P. D. Battle, T. C. Gibb, and S. Nixon, *J. Solid State Chem.* **79,** 75 (1989).
9. G. J. Long, T. E. Cranshaw, and G. Longworth, *Mössbauer Effect Reference and Data Journal* **6,** 42 (1983).
10. M. J. Johnson and W. I. F. David, Rutherford Appleton Laboratory No. 81/112 (1985).
11. S. Geller and A. E. Wood, *Acta Crystallogr.* **9,** 563 (1956).
12. D. B. Currie and M. T. Weller, *Acta Crystallogr., Sect. C* **47,** 696 (1991).
13. H. L. Yakel, *Acta. Crystallogr.* **8,** 394 (1955).
14. J. B. Machesney, R. C. Sherwood, and J. F. Potter, *J. Chem. Phys.* **43,** 1908 (1965).
15. V. N. Panyustikin, G. Pasquali, and G. Drickamer, *J. Chem. Phys.* **51,** 3305 (1969).
16. J. B. Torrance and P. Lacorro, *J. Solid State Chem.* **90,** 168 (1991).
17. A. Wattiaux, L. Fournes, A. Demauges, N. Bernaben, J. C. Grenier, and M. Pouchard, *Solid State Commun.* **77,** 489 (1991).
18. B. C. Tofield, C. Greaves, and B. E. F. Fender, *Mater. Res. Bull.* **10,** 737 (1975).
19. M. Harder and H. K. Muller-Buschbaum, *Z. Anorg. Allg. Chem.* **464,** 169 (1980).
20. Y. Takeda, K. Kanno, T. Takeda, O. Yamamoto, M. Takano, N. Nakayama, and Y. Bando, *J. Solid State Chem.* **63,** 237 (1986).
21. J. Mizusaki, M. Okayasu, S. Yamauchi, and K. Fueki, *J. Solid State Chem.* **99,** 166 (1992).
22. J. C. Grenier, J. Dournet, H. Pouchard, and P. Hagenmuller, *Mater. Res. Bull.* **11,** 1219 (1976).
23. P. D. Battle, T. C. Gibb, and P. Lightfoot, *J. Solid State Chem.* **84,** 237 (1990)
24. I. D. Brown and D. Aldermatt, *Acta Crystallogr., Sect. B* **41,** 244 (1985).